Received October 21, 2020, accepted October 24, 2020, date of publication October 27, 2020, date of current version November 11, 2020.
Digital Object Identifier 10.1109/ACCESS.2020.3034273

Study on Novel Bidirectional AC-DC Converter Circuit of the Wireless Charging for Portable Devices

ZHONGXIAN WANG[1,2], YONG SHI[1], AND TAO MENG[1], (Member, IEEE)
[1]School of Mechanical and Electrical Engineering, Heilongjiang University, Harbin 150080, China
[2]EMC Laboratory, Missouri University of Science and Technology (formerly known as University of Missouri-Rolla), Rolla, MO 65401, USA
Corresponding author: Zhongxian Wang (wangzhongxian@hlju.edu.cn)

This work was supported in part by the National Natural Science Foundation of China under Grant 51677056 and Grant 61703147, in part by the Natural Science Foundation of Heilongjiang Province under Grant E2016052, in part by the Heilongjiang University Fundamental Research Funds for the Heilongjiang Province Universities of China under Grant KJCX201916 and Grant RCYJTD201802, and in part by the Innovation Talent Research Special Foundations of Harbin Science and Technology Bureau of China under Grant 2016RQQXJ107.

ABSTRACT In this paper, a novel symmetrical topology for the small power high frequency bidirectional AC-DC converter has been proposed, which is applied to the bi-directional wireless power transmission system based on the magnetic coupling resonance. It has dual functions of the inverter and rectifier. The research is mainly reflected in the following aspects: First, based on analyzing the principle of the wireless power bidirectional transmission technology, the operation mechanism of the topology circuit is analyzed emphatically. Second, the feasibility of the designed converter is verified by the simulation of the PSPICE software. Third, the hardware system has been operated at 200 kHz in the modes of the constant current, the constant voltage and the constant resistance, respectively. The results show the maximal output power of the designed circuit is 7.8 W, meeting the design requirement. This circuit has the advantages of the simple circuit structure and simple control. It's suitable for the bidirectional wireless power charging of the small power portable devices.

INDEX TERMS AC-DC converter, bi-directional, magnetic resonance coupling, portable device, wireless power charging.

I. INTRODUCTION

The development of the wireless power transmission technology makes the development of the public mobile charging equipment possible. To some extent, it drives the development of the infrastructure [1]–[3]. With the widespread use of the portable devices (such as mobile phones, cameras, tablets, etc.), the wireless charging technology for the portable devices has become the research hotspots in the academic and industrial fields [4]–[9]. In this field, most of the current researches focus on the unidirectional transmission system, such as, the electrical power can only be transmitted to the portable devices through the power supply group. It has caused lots of inconveniences for the travelers. However, some power supply groups and mobile hand generators can also play an emergency role, which need rely on the power supply group. Some devices can charge between the portable devices through the Buck/Boost topology circuit, which need rely on the connection line [10]. Therefore, it is necessary to study the bidirectional wireless charging technology for the portable devices.

The circuit of the traditional bidirectional wireless charging system is composed of a fully controlled H bridge circuit and a resonant network [11], [12], which mainly used in the electric vehicle industry [13], [14]. It is well known, the full controlled H Bridge circuit produces more harmonic pollutions during the turn-on and turn-off of the power semiconductor devices, which needs the higher requirement for the latter EMI filter circuit and resonant network [15]. Moreover, the control method of the fully controlled H bridge circuit is relatively complex and tedious [16]. A bypass rectifier diode is added to the switching element to realize the wireless charging function between the portable devices, but the situation is without considering the charging of the power supply group to the portable device, and the maximal output power is 2.5 W [17]. For the small power portable devices, the full

The associate editor coordinating the review of this manuscript and approving it for publication was Zhilei Yao.

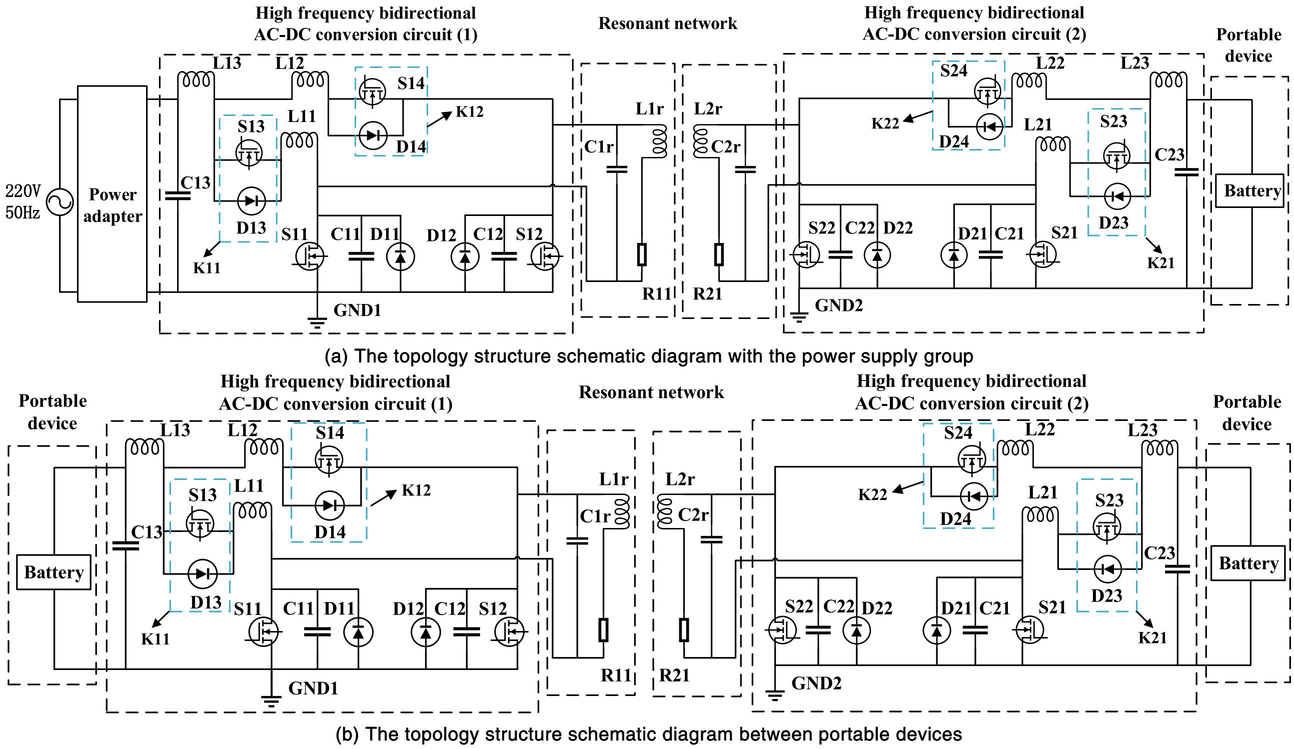

(a) The topology structure schematic diagram with the power supply group

(b) The topology structure schematic diagram between portable devices

FIGURE 1. **The topology structure schematic diagrams of bi-directional charging for wireless power.**

controlled H bridge converter not only has more energy loss, but also the volume is relatively large. Therefore, it is not suitable for the bidirectional wireless charging between the portable devices.

In order to overcome the prior art problems mentioned above, this paper is dedicated to solve the problem of the single and limited charging mode for the intelligent portable devices and other problems based on the former study [18]. A novel symmetrical topology circuit has been presented for the small power bidirectional wireless charging based on the magnetic coupling resonance, which has dual functions of the inverter and rectifier. It can not only realize itself as the charging terminal of the wireless power, but also realize itself as the power supply end of the wireless power to charge other portable devices when the situation is without the power supply group. It can be charged if only two people or two portable devices touch lightly together. And, the turn-on and turn-off times of the power semiconductor devices have been reduced. The research is aimed to reduce the volume of the device, improve the maximal output power and the compatibility of the device.

II. CIRCUIT TOPOLOGY AND PRINCIPLE

A. CIRCUIT TOPOLOGY

As shown in Fig. 1, the topology structure of the bidirectional wireless charging circuit is mainly composed of the high frequency bidirectional AC-DC converter and the resonant network. Among them, the high frequency bidirectional AC-DC converter is the main research object in this paper, and the PP structure is selected in the resonant network to improve the maximal output power. K_{11}, K_{12}, K_{21}, K_{22} are the control circuits of the operation state, which can be used as the common switch parallel diode structure, two diode parallel structure or the power electronic device parallel diode structure, as shown in Fig. 2. In this paper, the operation mode of the control circuits is described in Fig. 2(c).

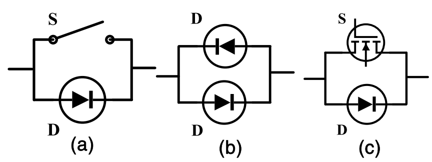

FIGURE 2. **Three kinds of control structures of K11, K12, K21, K22. (a) Switch parallel diode. (b) Two diodes are in parallel. (c) Power electronic device parallel diode.**

The topology structure of the high frequency bidirectional AC-DC converter is symmetrical, which has the inverter mode (discharge) and the rectifier mode (charge). In order to descript the operation principle, the symbols in Fig. 1 are simplified, as shown in Table 1. L_3 and C_3 make up the LC filter circuit, which has a filtering effect on the input and output. By controlling the turn-on and turn-off of 4 high frequency power switching tubes, the circuit can be controlled in the inverter mode or rectifier mode.

B. INVERTER OPERATION MODE

The driving signals are triggered by S_1 and S_2 in the high frequency bidirectional AC-DC conversion circuit. S_1 and

TABLE 1. Symbols description and its simplification.

Original symbols	Simplified symbols	Description
S_{11}, S_{21}	S_1	High frequency power switch tubes
S_{12}, S_{22}	S_2	High frequency power switch tubes
S_{13}, S_{23}	S_3	High frequency power switch tubes
S_{14}, S_{24}	S_4	High frequency power switch tubes
L_{11}, L_{21}	L_1	High frequency choke inductances
L_{12}, L_{22}	L_2	High frequency choke inductances
L_{13}, L_{23}	L_3	Input and output filter inductances
C_{11}, C_{21}	C_1	Bypass capacitors of S_1
C_{12}, C_{22}	C_2	Bypass capacitors of S_2
C_{13}, C_{23}	C_3	Input and output filter capacitors
D_{11}, D_{21}	D_1	Free-wheeling diodes of S_1
D_{12}, D_{22}	D_2	Free-wheeling diodes of S_2
D_{13}, D_{23}	D_3	The conduction diodes
D_{14}, D_{24}	D_4	The conduction diodes
L_{1r}, L_{2r}	L_r	Resonant inductances
C_{1r}, C_{2r}	C_r	Resonant capacitors
R_{11}, R_{21}	R_1	The equivalent internal resistance of L_r
K_{11}, K_{21}	K_1	Control circuits of operation state
K_{12}, K_{22}	K_2	Control circuits of operation state

S_2 are the complementary conduction to each other, and the duty cycle is 50%. At the same time, S_3 and S_4 operate in the shutdown mode. U_{DC} supplies the power for the AC-DC topology circuits. When S_1 and S_2 are alternately turned on, the AC-DC topology operates in the inverter mode. The high frequency sine wave is generated at both ends of L_r and C_r. The schematic diagram of the equivalent circuit structure of the high frequency bidirectional AC-DC converter operating in the inverter mode is shown in Fig. 3. The current direction has been marked in the graph.

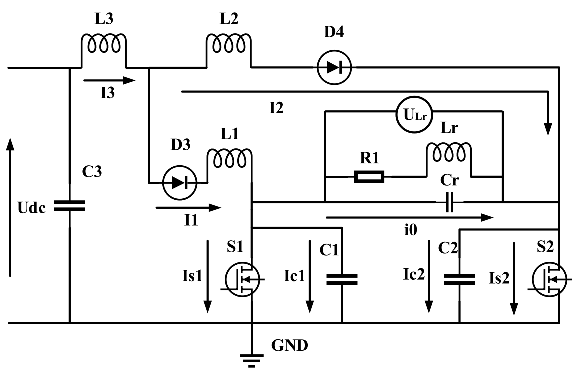

FIGURE 3. Schematic diagram of the equivalent circuit in inverter mode.

In Fig. 3, the impedances of the inductances L_1 and L_2 are large enough, so the current fluctuations passing through L_1 and L_2 are very small. In order to descript the inverter operation mode, the symbols in Fig. 3 are listed, as shown in Table 2.

According to the analysis of the zero voltage switching and zero current switching, the maximum output voltage U_{LrMAX} of the resonant element is,

$$U_{LrMAX} = 3.562U_{dc} \tag{1}$$

TABLE 2. Symbols description in inverter operation mode.

Original symbols	Description
I_1	The current of L_1
I_{S1}	The current of S_1
I_{C1}	The current of C_1
I_2	The current of L_2
I_{S2}	The current of S_2
I_{C2}	The current of C_2
i_0	The resonant current of L_r and C_r
I_3	The current of L_3, which is approximately equal to the input current
U_{dc}	The input voltage

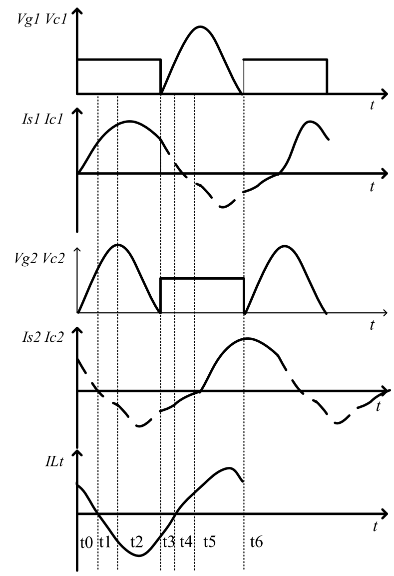

FIGURE 4. The operation waveform of the inverter state in one period.

Fig. 4 shows the operation waveform of the inverter state in one period. According to the Fig. 4, the specific operating process of the Fig. 3 is as follows:

1) S_1 is switched from the close state to the open state, S_2 is switched from the open state to the close state.

In t_0- t_1: on the side of S_1, I_{S1} begins to rise, and i_0 begins to decrease due to $I_{S1} = I_1$-i_0. On the side of S_2, I_{S2} is reduced and I_{C2} is raised. At this time, C_2 is charged and the charging current is that $I_{C2} = I_2 + i_0$. C_2 is gradually filled with the electricity. The load voltage drops to 0 V and then goes to the next stage.

In t_1- t_2: the current I_2 flows into C_2, L_r and C_r, respectively. The resonant current i_0 will be charging over. Currently, $I_1 = I_{C1}+i_0$. When C_2 is full of the electricity, $i_0 = I_2$.

In t_2–t_3: C_2 begins to discharge and then flows into L_r, C_r, R_1 and S_1. The voltage on C_2 begins to decrease.

2) S_1 is switched from the open state to the close state, S_2 is switched from the close state to the open state.

In t_3–t_4: on the side of S_2, I_{S2} begins to rise, and i_0 begins to decrease due to $I_{S2} = I_2$-i_0. On the side of S_1, I_{S1} is reduced and I_{C1} is raised. At this time, C_1 is charged and the charging current is that $I_{C1} = I_1 + i_0$. C_1 is gradually filled with the electricity. The load voltage drops to 0 V and then goes to the next stage.

In t_4–t_5: the current I_1 flows into C_1, L_r and C_r, respectively. The resonant current i_0 will be charging over. Currently, $I_1 = I_{C1} + i_0$. When the capacitor C_2 is full of the electricity, $i_0 = I_1$.

In t_5–t_6: C_1 begins to discharge and then flows into L_r, C_r, R_1 and S_2. The voltage on C_1 begins to decrease.

C. RECTIFIER OPERATION MODE

The driving signals are triggered by S_3 and S_4 in the high frequency bidirectional AC-DC conversion circuit. S_3 and S_4 are the complementary conduction to each other, and the duty cycle is 50%. At the same time, S_1 and S_2 operate in the shutdown mode. The AC-side input power is from L_r and C_r, which supplies to the AC-DC topology circuits. When S_3 and S_4 are alternately turned on, the AC-DC topology operates in the rectifier mode. Then the DC current is generated at RL of the output side. The schematic diagram of the equivalent circuit structure of the high frequency bidirectional AC-DC converter operating in the rectifier mode is shown in Fig. 5.

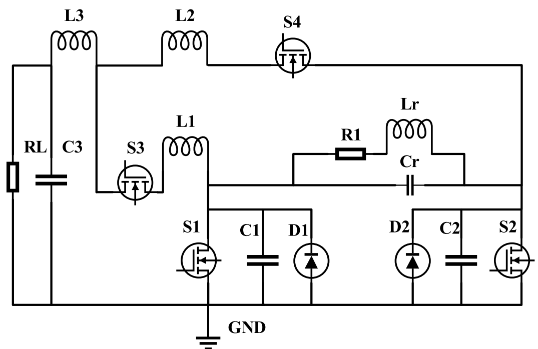

FIGURE 5. Schematic diagram of the equivalent circuit in rectifier mode.

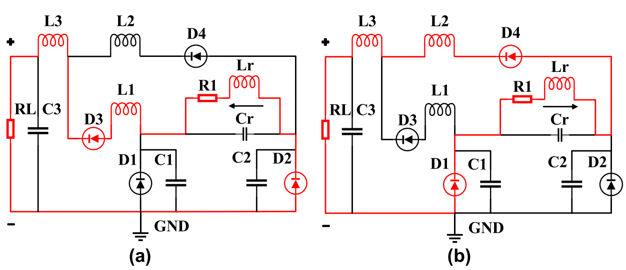

FIGURE 6. Current flow diagrams of the simplified equivalent circuit.

The high frequency sine wave is coupled to the receiving coil by the transmitting coil through the magnetic coupling wireless power transmission mode. L_r and C_r are the resonant elements which couple the same frequency sine wave in the receiving coil. At this point, S_1 and S_2 operate in the shutdown mode, S_3 and S_4 are alternately turned on. The schematic diagram of the simplified equivalent circuit is shown in Fig. 6.

D_3 and D_4 can be used to replace S_3 and S_4, which can realize the full wave rectification in a complete period.

In Fig. 6, the circuit is like the single-phase full bridge uncontrolled rectifier circuit, so the relationship before the filter between the input and the output voltage is,

$$U_{dc} = 0.9U_{Lr} \tag{2}$$

where, U_{dc} is the output DC voltage of the circuit, U_{Lr} is the input voltage RMS of the resonant element L_r.

As shown in Fig. 5 and Fig. 6, the specific operating process is as follows:

1) S_3 is switched from the close state to the open state, S_4 is switched from the open state to the close state, as shown in Fig. 6(a). Suppose that the current of L_r is positive to the left, the current of the positive half cycle flows through L_r, L_1, D_3, L_3, R_L and D_2. Then it finally returns to L_r. The current flow can be seen in the red thick line.

2) S_4 is switched from the close state to the open state, S_3 is switched from the open state to the close state, as shown in Fig. 6(b). Suppose that the current of L_r is negative to the right, the current of the negative half cycle flows through L_r, D_4, L_2, L_3, R_L and D_1. Then it finally returns to L_r. The current flow can be seen in the red thick line.

Therefore, in a complete period, it can be rectified and filtered through two branches, and the power is supplied to the load.

In conclusion, this novel bidirectional AC-DC topology circuit can work normally both in the inverter mode and in the rectifier mode in theory.

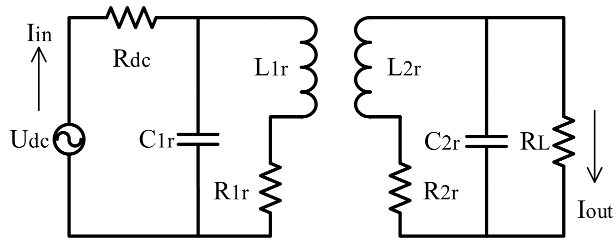

FIGURE 7. The equivalent model of the system.

D. SYSTEM TRANSMISSION EFFICIENCE

Fig. 7 shows the equivalent model of the wireless power transmission system. Due to the symmetrical structure of the bidirectional AC-DC converter, the parameters of the receiver and transmitter are the same. U_{dc} is an equivalent voltage source, R_{dc} is an internal resistance of the equivalent power source, $R_{1r} = R_{2r} = R_r$ are the equivalent internal resistances of the resonant circuit, $L_{1r} = L_{2r} = L_r$ are the coil self inductance, $C_{1r} = C_{2r} = C_r$ are the resonant capacitance, M is the mutual inductance between the resonant coils, R_L is a load resistance, i_{1r} and i_{2r} are the primary and secondary side currents respectively, I_{in} is the RMS of the input current, I_{out} is the RMS of the output DC current.

When the circuit is the optimal resonant operation state, the KVL equations of the primary and secondary side are obtained,

$$\begin{cases} i_{1r}Z_{1r} - j\omega MI_{2r} = U_{dc} \\ i_{2r}Z_{2r} - j\omega MI_{1r} = 0 \end{cases} \quad (3)$$

where,

ω is the operating angle frequency of the inverter circuit.

The primary and secondary impedances Z_{1r}, Z_{2r} are,

$$\begin{cases} Z_{1r} = R_{dc} + j\dfrac{1}{\omega C_{1r}} // (R_{1r} + j\omega L_{1r}) \\ Z_{2r} = R_L + j\dfrac{1}{\omega C_{2r}} // (R_{2r} + j\omega L_{2r}) \end{cases} \quad (4)$$

In the optimal resonant state, the reactive power is not considered. When R_r is far less than ωL_r, the equation (4) is simplified as,

$$\begin{cases} Z_{1r} = R_{dc} + \dfrac{L_r}{C_r R_r} \\ Z_{2r} = R_L + \dfrac{L_r}{C_r R_r} \end{cases} \quad (5)$$

Assuming that the mapping impedance Z_s is,

$$Z_s = \frac{(\omega M)^2}{Z_{2r}} \quad (6)$$

Therefore, when $L_r/(C_r R_r) = LCR$, the input current I_{in} and the output current I_{out} are,

$$\begin{cases} I_{in} = \dfrac{U_{dc}}{Z_{1r} + Z_s} = \dfrac{U_{dc}}{R_{dc} + LCR + \dfrac{(\omega M)^2}{LCR + R_L}} \\ I_{out} = \dfrac{4}{\pi}\dfrac{j\omega M \cdot U_{dc}}{Z_{1r} Z_{2r}} = \dfrac{4}{\pi}\dfrac{j\omega M \cdot U_{dc}}{(R_{dc} + LCR)(R_L + LCR)} \end{cases} \quad (7)$$

The input power is,

$$P_{in} = \left(\frac{U_{dc}}{R_{dc} + LCR + \frac{(\omega M)^2}{LCR + R_L}}\right)^2 \left(LCR + \frac{(\omega M)^2}{LCR + R_L}\right) \quad (8)$$

The output power is,

$$P_{out} = \left(\frac{4}{\pi}\frac{\omega M \cdot U_{dc}}{(R_{dc} + LCR)(R_L + LCR) + (\omega M)^2}\right)^2 R_L \quad (9)$$

In the ideal state, when the power transmission efficiency of the inverter side meets ZVS, ZDS and other conditions, $\eta_1 = 1$. Then, the system transmission efficiency η is,

$$\eta = \eta_1 \eta_2 = \eta_2 = \frac{1.62}{1 + \frac{L_r}{C_r R_r R_L} + \frac{\frac{L_r}{C_r R_r}\left(\frac{L_r}{C_r R_r} + R_L\right)^2}{R_L (\omega M)^2}} \quad (10)$$

The system transmission efficiency η is derived from R_L,

$$\frac{\partial \eta}{\partial R_L} = 0 \quad (11)$$

When the equation (11) is 0, the system transmission efficiency is the maximum, and the optimal load R_{LM} is,

$$R_{LM} = \sqrt{\left(\frac{L_r}{C_r R_r}\right)^2 + (\omega M)^2} \quad (12)$$

III. SIMULATION ANALYSIS

Fig. 8 shows the whole schematic diagram of the bidirectional wireless power charging system, in which the dotted line is a resonant circuit. While the Buck/Boost circuit is used as the auxiliary circuit of the voltage rise and fall in the system, it will not be discussed in this paper.

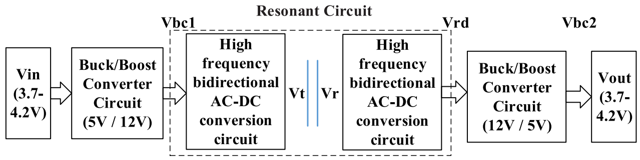

FIGURE 8. The overall schematic diagram of the bidirectional wireless power charging system.

In Fig. 8, V_{in} is the input DC voltage of the system, which ranges from 3.7 V to 4.2 V; V_{bc1} and V_{bc2} are the output DC voltage of the Buck/Boost circuit respectively, which converts 5 V to 12 V or 12 V to 5 V; V_t is the output AC voltage RMS of the transmitter; V_r is the input AC voltage RMS of the receiver; V_{rd} is the output DC voltage of the rectifier device; V_{out} is the output DC voltage of the system, which ranges from 3.7 V to 4.2 V.

By controlling the operation modes of the switch tubes, the left side of the bidirectional AC-DC circuit is used as the inverter, and the right side of the bidirectional AC-DC circuit is used as the rectifier. In order to facilitate the simulation, S_3 and S_4 are replaced by the diodes, seen in Fig. 3 and Fig. 6.

The input DC voltage of the bidirectional AC-DC circuit is 12 V. For the magnetic coupling resonance mode, it is theoretically considered that when the resonant frequencies of the transmitting coil and the receiving coil are the same, the transmission efficiency can reach 100%, and the coupling coefficient is 1. Considering the actual operation, the wireless power transmission system has a deviation, so the coupling coefficient of L_{1r} and L_{2r} is set to 0.3. The designed bidirectional AC-DC converter will apply to the small power portable devices, which need conform to the Qi standard. Considering the operation efficiency, the operation frequency is 200 kHz. And, the duty cycle of the switch tubes is 50%. The load R_L is 7.83 Ω. Then, the voltage waveform of transmitter coil is shown in Fig. 9.

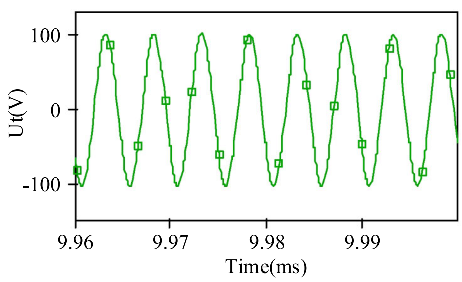

FIGURE 9. When R_L is 7.83 Ω, the voltage waveform of transmitter coil.

It can be seen from Fig. 9 that the peak voltage is about 100 V which is more than 8 times of the DC bus voltage.

There are the good sine and low harmonic content. The simulation is basically the same as the bidirectional AC-DC converter as the inverter.

When R_L is 7.83 Ω, the voltage waveform of the receiver coil is shown in Fig. 10.

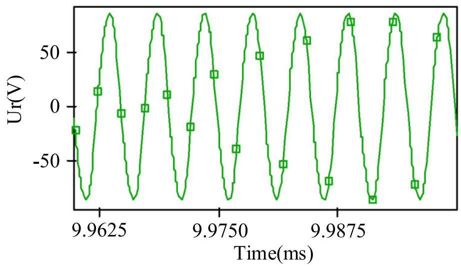

FIGURE 10. When RL is 7.83 Ω, the voltage waveform of receiver coil.

It can be seen from Fig. 10 that the peak voltage is about 95 V which is lower than the transmitter voltage. Also, there are the good sine and low harmonic content. The simulation is basically the same as the bidirectional AC-DC converter as the rectifier.

When the load is 7.83 Ω and the other conditions are constant, the output voltage and current waveforms are shown in Fig. 11.

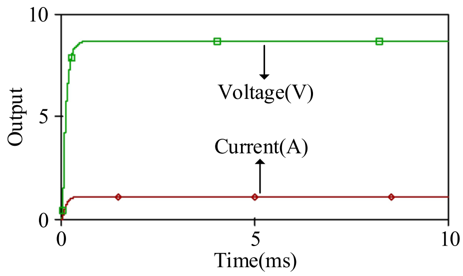

FIGURE 11. When RL is 7.83 Ω, the output voltage and current waveform of system.

As shown in Fig. 11, the output voltage of the system is smooth and stable at 8.5 V, and the output current of the system is smooth and stable at 1.13 A. The operation efficiency is 53.4% due to the low coupling coefficient.

Through the above simulation analysis, the bidirectional AC-DC converter can operate independently. Moreover, it can switch between the inverter and the rectifier according to the different control modes of the switch tubes. A bidirectional chopper circuit can be added between the DC power supply side and the bidirectional AC-DC converter. It makes the bidirectional output voltage more stable, so the voltage regulation and voltage stabilization can be achieved.

IV. CIRCUIT PARAMETERS

In the test of the hardware, the resonant coil conforms to the Qi standard, as shown in Fig. 12. The specific parameters of the resonant coil are as follows: the inner diameter of the resonant coil is 5 mm, the outer diameter is 23 mm, and

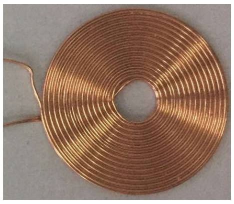

FIGURE 12. Resonant coil with Qi standard.

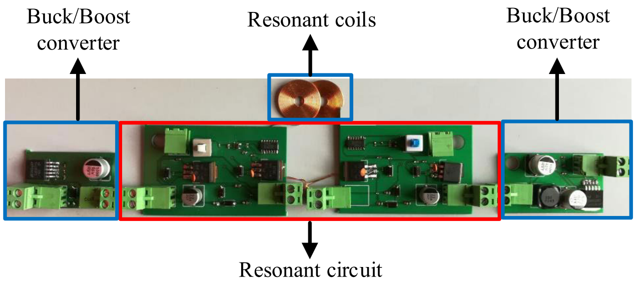

FIGURE 13. Prototype of bi-directional wireless charging circuit.

the thickness is 1 mm. The actual circuit of the bidirectional wireless charging is shown in Fig. 13. It mainly composed of the resonant coil, the Buck/Boost circuit and the resonant circuit which have been marked in the graph. Among them, the resonant circuit consists of two circuits with the same topological structure. Each circuit has the dual functions of the transmitter and the receiver.

In the system, the DC input voltage is 5 V, the output voltage is 5 V, the output power is 5 W, the resonant frequency is 200 kHz, the duty cycle is 0.5, and the load resistance R_L is 7.83 Ω.

If the bypass capacitor of the switch tube can meet the operating conditions of ZVS and ZDS of the system, then,

$$C = \frac{4}{(1+\frac{\pi^2}{4})\cdot\pi\cdot 2\pi f\cdot R} \tag{13}$$

According to the equation (13), $C_1 = C_2 = C_3 =$ 37.38 nF.

The high frequency choke inductance and the filter inductance are,

$$L \geq \frac{R}{(2\pi f)^2 \cdot C} \tag{14}$$

It can be seen from the equation (14), $L \geq 132.65\ \mu$H. And the actual inductance value should be greater than the calculated value. However, if L is too large, not only the dynamic adjustment becomes slower, but also the filtering effect with the high frequency will be worse. So, $L_1 = L_2 = L_3 = 150\ \mu$H.

According to the resonance frequency formula, the resonant capacitor is,

$$C_r = \left(\frac{1}{2\pi f}\right)^2 \cdot \frac{1}{L_r} \tag{15}$$

TABLE 3. Circuit parameters.

Item	Model number & parameter
PCB size of the resonant circuit	67 mm×53 mm
Driver IC	LTC6900
MOSFETs	IRF840N
Schottky diode	1N5822
Input voltage *Vin*	5 V
Output voltage *Vout*	5 V
Output power *Pout*	5 W
Self-inductances *Lr*	8 / 8 μH
Resonant capacitors *Cr*	79.16 / 79.16 nF
Switching frequency for resonant circuit	200 kHz
Resonant frequency for resonant circuit	200 kHz
High frequency choke inductances L_1, L_2 and filter inductance L_3	150 μH
Bypass capacitors C_1, C_2 and filter capacitor C_3	37.38 nF

Set $Lr = 8\ \mu$H,. according to the equation (15), the resonant capacitance $Cr = 79.16$ nF.

In Table 3, it shows the specific parameters of the components of the bidirectional wireless charging circuit.

V. EXPERIMENTAL RESULTS

In this experiment, the input voltage of the system is 5 V and the output voltage of the system is 5 V. The Buck/Boost circuit adopts the fixed duty cycle modulation mode. When it is used as a Buck circuit, the output voltage is 5 V. When it is used as a Boost circuit, the output voltage is 12 V. The resonant circuit with the bidirectional wireless charging adopts the fixed frequency modulation mode. The power supply adopts the model DF1743003C, which provides the DC input voltage to the system. The load adopts the model IT8512+, which can be set at the constant current (CC), the constant voltage (CV) and the constant resistance (CR). When the CC mode is applied, the current is set to 0.5 A. When the CV mode is applied, the voltage is set to 5 V. When the CR mode is applied, the resistance is set to 5 Ω. The oscilloscope uses the Tektronix TDS2012C, which is used to measure the AC voltage waveform, the AC current waveform and the DC voltage waveform, respectively.

Fig. 14 shows the voltage waveform of the resonant coil of the transmitting and receiving terminals at no-load time. The sine is good and the frequency is 200 kHz. When the coil spacing is 2 mm, the RMS voltage of the transmitting coil is 17.8 V, and the coupling RMS voltage of the receiving coil is 19.5 V, as shown in Fig. 14(a). When the coil spacing is 15 mm, the RMS voltage of the transmitting coil is 21.6 V, and the coupling RMS voltage of the receiving coil is 13.2 V, as shown in Fig. 14(b). Fig. 15 shows the current waveform of the resonant coil of the transmitting and receiving terminals at no-load time. The sine is good and the frequency is 200 kHz. When the coil spacing is 2 mm, the RMS current of the transmitting coil is 84.7 mA, and the coupling RMS current of the receiving coil is 77.5 mA, as shown in Fig. 15(a). When the coil spacing is 15mm, the RMS current of the transmitting coil is 116 mA, and the coupling RMS current of the receiving coil is 64.8 mA, as shown in Fig. 15(b). Fig. 16 shows the output voltage waveform after the rectifier and filtering of the receiver at no-load time. The ripple is less than 3%. When the coil spacing is 2 mm, the output DC RMS voltage is 56.3 V and the peak voltage is 1.6 V, as shown in Fig. 16(a). When the coil spacing is 15 mm, the output DC RMS voltage is 42.2 V and the peak voltage is 0.8 V, as shown in Fig. 16(b).

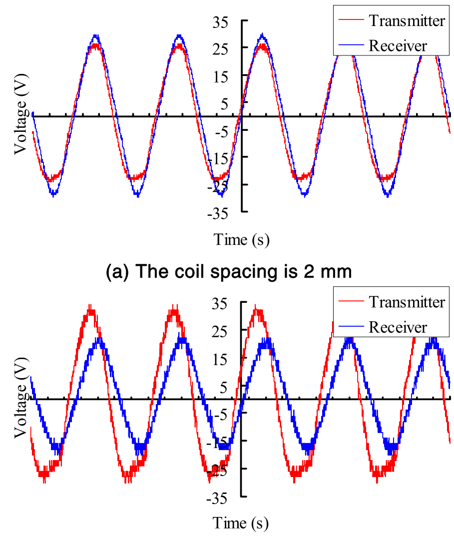

(a) The coil spacing is 2 mm
(b) The coil spacing is 15 mm

FIGURE 14. The voltage waveforms of transmitter and receiver at no-load time.

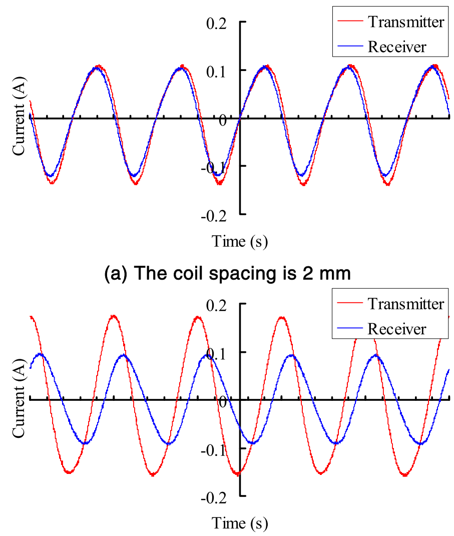

(a) The coil spacing is 2 mm
(b) The coil spacing is 15 mm

FIGURE 15. The current waveforms of transmitter and receiver at no-load time.

Fig. 17 shows the voltage waveform of the resonant coil of the transmitting and receiving terminals at the load (CV mode). The sine degree is good and the frequency is 200 kHz. When the coil spacing is 2 mm, the RMS voltage of the transmitting coil is 15.9 V, and the coupling RMS voltage of the receiving coil is 15.1 V, as shown in Fig. 17(a).

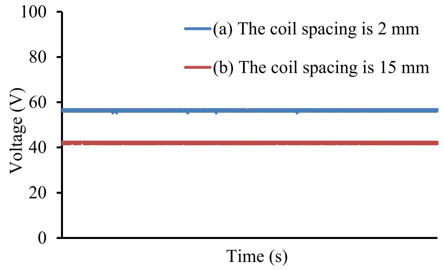

FIGURE 16. **The voltage waveforms of the receiver after the filter at no-load time.**

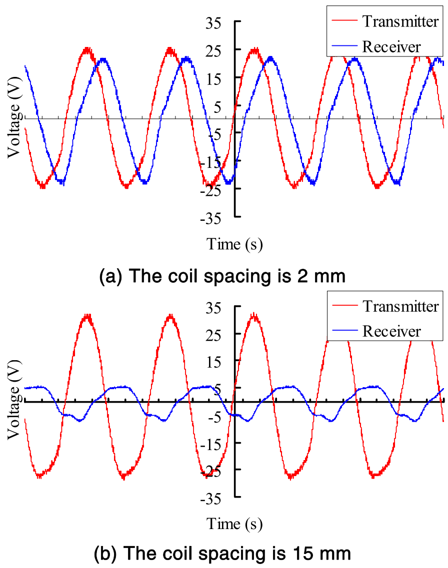

FIGURE 17. **The voltage waveforms of transmitter and receiver at load time (CV mode).**

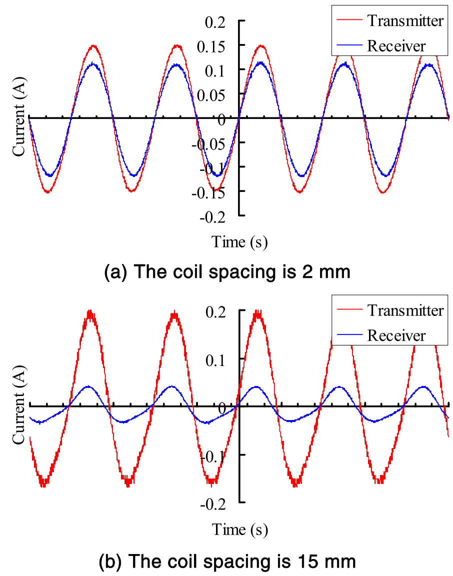

FIGURE 18. **The current waveforms of transmitter and receiver at load time (CV mode).**

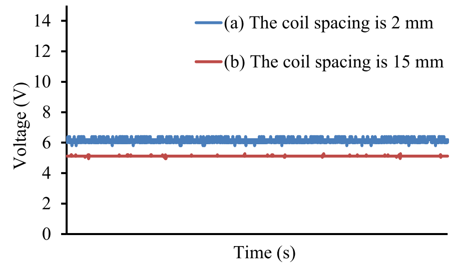

FIGURE 19. **The voltage waveforms of the receiver after the filter at load time (CV mode).**

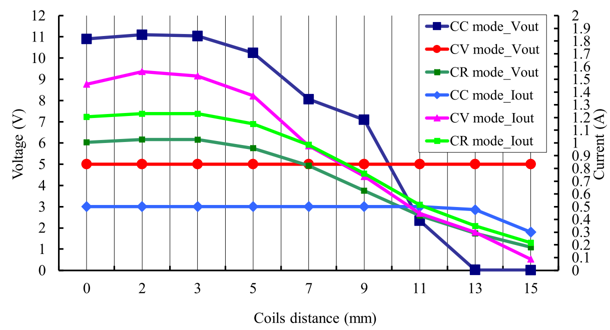

FIGURE 20. **When the coils spacing is different, the system output DC voltage and DC current curves of different operation modes.**

When the coil spacing is 15 mm, the RMS voltage of the transmitting coil is 21.5 V, and the coupling RMS voltage of the receiving coil is 4.46 V, as shown in Fig. 17(b). Fig. 18 shows the current waveform of the resonant coil of the transmitting and receiving terminals at the load (CV mode). The sine degree is good and the frequency is 200 kHz. When the coil spacing is 2 mm, the RMS current of the transmitting coil is 106 mA, and the coupling RMS current of the receiving coil is 68.1 mA, as shown in Fig. 18(a). When the coil spacing is 15mm, the RMS current of the transmitting coil is 122 mA, and the coupling RMS current of the receiving coil is 24.9 mA, as shown in Fig. 18(b). Fig. 19 shows the output voltage waveform after the rectifier and filtering of the receiver at the load (CV mode). The ripple is less than 10%. When the coil spacing is 2 mm, the DC output RMS voltage is 6.16 V and the peak value is 0.6 V, as shown in Fig. 19(a). When the coil spacing is 15 mm, the DC output RMS voltage is 5.12 V and the peak value is 0.32 V, as shown in Fig. 19(b).

Fig. 20 shows the DC voltage and current of the system in the different operating modes when the coil spacing is different. When the system operates in the CC mode, the output DC current is 0.5 A and the coil spacing ranges from 0 to 9 mm, its output DC voltage will be greater than 5 V and the maximum is 11.1 V. When the coil spacing is 11 mm, the output DC voltage is 2.34 V. When the system operates in the CV mode, the output DC voltage is 5 V and the coil spacing ranges from 0 to 9 mm, its output DC current is greater than 0.5 A and the maximum is 1.56 A. When the coil spacing is 11 mm, the output DC current is 0.45 A. When the system operates in the CR mode and the coil spacing ranges from 0 to 7 mm,

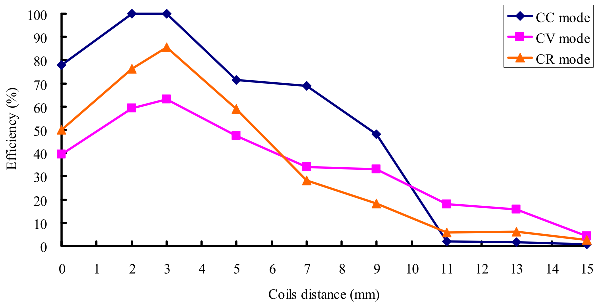

FIGURE 21. Resonance coil conversion efficiency under different operation mode.

its output DC voltage will be greater than 5 V and its output DC current is greater than 0.5 A. When the coil spacing is 9 mm, the output DC voltage is 3.75 V and the output DC current is 0.76 A. When the coil spacing is 11 mm, the output DC voltage is 2.58 V and the output DC current is 0.51 A.

Fig. 21 shows the conversion efficiency of the resonant coil under the different operating modes. It can be seen from the results, the conversion efficiency of the CC mode is obviously higher than the CV and CR modes. When the coil spacing ranges from 2 mm to 3 mm, the conversion efficiency of the CC mode is close to be 100%. When the coil spacing is 9 mm, the conversion efficiency of the CC mode is 48.22%. When the coil spacing is 3 mm, the highest conversion efficiency of the CV mode is 63.2%. When the coil spacing is 3 mm, the highest conversion efficiency of the CR mode is 85.66%. Fig. 22 shows the conversion efficiency of the resonant circuit under the different operating modes. It can be seen from the results, the overall conversion efficiency of the resonant circuit in three operating modes is not high, and the maximum efficiency is about 40%.

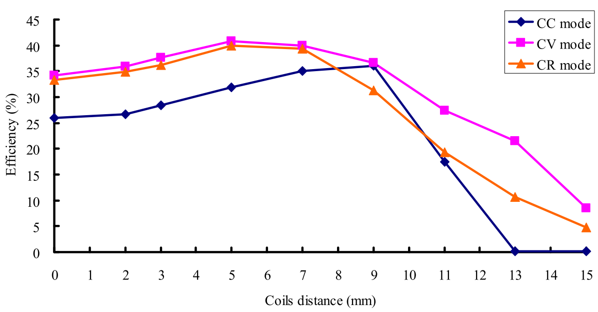

FIGURE 22. Resonance circuit conversion efficiency under different operation mode.

In order to verify the advantages of the proposed circuit, compare with the existing research [17] in this area, the results are shown in Table 4.

According to the data analysis, the designed bi-directional AC-DC converter topology circuit can not only realize the inverter function, but also realize the rectifier function. The numbers of the controlled switch tube of the proposed circuit is less than the existing research. The proposed circuit

TABLE 4. Comparative results.

The performance index	The proposed circuit	The existing research
The size of the resonant circuit	67 ×53 mm	None
The numbers of the rectifier	1	1
The numbers of the inverter	1	1
The numbers of the switch tube	8	8
The numbers of the controlled switch tube	4	8
The inner diameter of the coil	5 mm	32 mm
The outer diameter of the coil	23 mm	21.7 mm
The thickness of the coil	1 mm	Double-layer
The size of the ferrite square plate	None	34 × 34 mm
The operation frequency	200 kHz	205 kHz
The maximal output power	7.8 W / 2 mm air gap	2.5 W / 2 mm air gap
The efficiency	About 40%	About 70%
Cost	Low	None

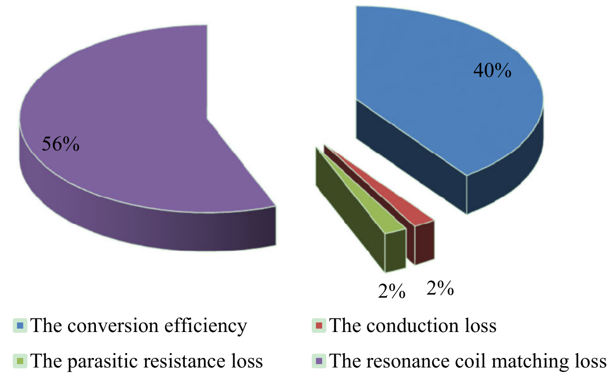

FIGURE 23. The power distribution of the device.

does not adopt the ferrite square plate. When the resonant frequency is 200 kHz, the coil spacing ranges from 0 to 5 mm, no matter in which mode, the output power of the proposed circuit is greater than 5 W. The maximal output power can reach 7.8 W which is larger than the existing research. And most of performance indexes of the proposed circuit are high, which meet the design requirements.

However, the conversion efficiency of the proposed resonant circuit is not perfect. The main reasons are as follows: (1) the turn-on voltage drop in the switch tube has the conduction loss; (2) the switch tube has a parasitic resistance which generates the loss; (3) the problem of the resonance coil matching. Fig. 23 shows the power distribution of the device. The result shows that the maximal loss is from the resonance coil matching. According to the equation (10) and the equation (12), when the ratio of Lr and Cr is about 49, and the optimal load is 7.83 Ω, the maximal efficiency is about 100% theoretically. However, the actual parameters of the resonant coil exist the error. The actual ratio of Lr and Cr is about 101.06 so that the optimal matching is not achieved.

VI. CONCLUSION

In this paper, the method of the software simulation and the hardware testing are combined. A novel bidirectional AC-DC converter topology has been designed. The inverter module and the rectifier module have been integrated, and the circuit has been controlled by 4 switch tubes. It can realize the bidirectional flow of the electric energy. After analyzing the converter theoretically, the feasibility of the designed bidirectional AC-DC converter has been verified by PSPICE software simulation analysis. Finally, in the test of the hardware system, the experimental results show that the designed bi-directional AC-DC converter has a dual function of the inverter and rectifier. When the resonance frequency is 200 kHz and the coil spacing is range from 0 to 5 mm, no matter in which mode, the output power is greater than 5 W, and the maximum output power can be 7.8 W. When the coil spacing is 2 mm and the output DC current is 0.5 A, the output DC voltage can up to be 11.1 V. When the coil spacing is 2 mm and the output DC voltage is 5 V, the output DC current can up to be 1.56 A. However, the overall conversion efficiency of the resonant circuit in the three operation modes is not high due to the low coupling coefficient and the bad resonance coil matching, other performance indexes present well.

REFERENCES

[1] X. Wei, Z. Wang, and H. Dai, "A critical review of wireless power transfer via strongly coupled magnetic resonances," *Energies*, vol. 7, no. 7, pp. 4316–4341, Jul. 2014.
[2] Z. Bi, T. Kan, C. C. Mi, Y. Zhang, Z. Zhao, and G. A. Keoleian, "A review of wireless power transfer for electric vehicles: Prospects to enhance sustainable mobility," *Appl. Energy*, vol. 179, pp. 413–425, Oct. 2016.
[3] S. D. Barman, A. W. Reza, N. Kumar, M. E. Karim, and A. B. Munir, "Wireless powering by magnetic resonant coupling: Recent trends in wireless power transfer system and its applications," *Renew. Sustain. Energy Rev.*, vol. 51, pp. 1525–1552, Nov. 2015.
[4] D. van Wageningen and T. Staring, "The Qi wireless power standard," in *Proc. 14th Int. Power Electron. Motion Control Conf. EPE-PEMC*, Ohrid, Macedonia, Sep. 2010, pp. S15–S25.
[5] E. Waffenschmidt, "Wireless power for mobile devices," in *Proc. IEEE 33rd Int. Telecommun. Energy Conf. (INTELEC)*, Amsterdam, The Netherlands, Oct. 2011, pp. 1–9.
[6] M. Galizzi, M. Caldara, V. Re, and A. Vitali, "A novel qi-standard compliant full-bridge wireless power charger for low power devices," in *Proc. IEEE Wireless Power Transf. (WPT)*, Perugia, Italy, May 2013, pp. 44–47.
[7] K. Takeno, "Wireless power transmission technology for mobile devices," *IEICE Electron. Express*, vol. 10, no. 21, 2013, Art. no. 20132010.
[8] Y. Zhang, Z. Zhao, K. Chen, and J. Fan, "Load characteristics of wireless power transfer system with different resonant types and resonator numbers," *AIP Adv.*, vol. 7, no. 5, Aug. 2017, Art. no. 056601.
[9] I. Sherman and T. Demri, "Bi-directional battery charging for coupled electronic devices," U.S. Patent 7 863 856 B2, Jan. 4, 2011.
[10] X. Shu, W. Xiao, and B. Zhang, "Wireless power supply for small household appliances using energy model," *IEEE Access*, vol. 6, pp. 69592–69602, 2018.
[11] U. K. Madawala and D. J. Thrimawithana, "Current sourced bi-directional inductive power transfer system," *IET Power Electron.*, vol. 4, no. 4, pp. 471–480, Apr. 2011.
[12] K. Chen, Z. Zhao, F. Liu, and L. Yuan, "Analysis of resonant topology for bi-directional wireless charging of electric vehicle," *Automat. Electr. Power Syst.*, vol. 41, no. 2, pp. 66–72, Feb. 2017.
[13] D. J. Thrimawithana, U. K. Madawala, A. Francis, and M. Neath, "Magnetic modeling of a high-power three phase bi-directional IPT system," in *Proc. 37th Annu. Conf. IEEE Ind. Electron. Soc. (IECON)*, Melbourne, VIC, Australia, Nov. 2011, pp. 1414–1419.
[14] L. Tan, Z. Zhang, Z. Zhang, B. Deng, M. Zhang, J. Li, and X. Huang, "A segmented power-efficiency coordinated control strategy for bidirectional wireless power transmission systems with variable structural parameters," *IEEE Access*, vol. 6, pp. 40289–40301, 2018.
[15] C. Song, H. Kim, Y. Kim, D. Kim, S. Jeong, Y. Cho, S. Lee, S. Ahn, and J. Kim, "EMI reduction methods in wireless power transfer system for drone electrical charger using tightly coupled three-phase resonant magnetic field," *IEEE Trans. Ind. Electron.*, vol. 65, no. 9, pp. 6839–6849, Sep. 2018.
[16] S. Kouro, P. Cortes, R. Vargas, U. Ammann, and J. Rodriguez, "Model predictive control—A simple and powerful method to control power converters," *IEEE Trans. Ind. Electron.*, vol. 56, no. 6, pp. 1826–1838, Jun. 2009.
[17] S. Miura, K. Nishijima, and T. Nabeshima, "Bi-directional wireless charging between portable devices," in *Proc. Int. Conf. Renew. Energy Res. Appl. (ICRERA)*, Madrid, Spain, Oct. 2013, pp. 775–778.
[18] Z. Wang, Y. Liu, Y. Wei, and Y. Song, "Study on electromagnetic characteristics of the magnetic coupling resonant coil for the wireless power transmission system," *J. Appl. Biomater. Funct. Mater.*, vol. 16, no. 1, pp. 140–149, Jan. 2018.

ZHONGXIAN WANG was born in Heilongjiang, China, in 1982. He received the B.S. degree in electrical engineering from the Harbin University of Science and Technology, Harbin, China, in 2004, and the M.S. degree in control and instrument engineering from Wonkwang University, Iksan, South Korea, in 2007.

He is currently a Senior Engineer with the School of Mechanical and Electrical Engineering, Heilongjiang University, Harbin. His research interests include high-frequency power conversion techniques, and wireless power transmission techniques and its applications.

YONG SHI was born in Hubei, China, in 1973. He received the B.S. and Ph.D. degrees in mechanical engineering from the Harbin Institute of Technology, Harbin, China, in 1995 and 2004, respectively.

He is a Professor with the School of Mechanical and Electrical Engineering, Heilongjiang University, Harbin. His research interests include mechanical design and automatic control.

TAO MENG (Member, IEEE) was born in Liaoning, China, in 1980. He received the B.S., M.S., and Ph.D. degrees in electrical engineering from the Harbin Institute of Technology, Harbin, China, in 2003, 2005, and 2010, respectively.

He is currently a Professor with the School of Mechanical and Electrical Engineering, Heilongjiang University. His research interests include power factor correction techniques, high frequency ac/dc and dc/dc conversion techniques, and magnetic integration techniques and its applications.